

Fatigue and Mechanical Behavior in Sintered ZrN Pellets: FY02

P. Peralta and I. Han

Arizona State University

Department of Mechanical and Aerospace Engineering

Tempe, AZ 85287-6106

Summary

The fatigue behavior and mechanical properties of sintered ZrN were studied and measured to evaluate the mechanisms that can compromise the structural stability of fuels during transmutation, with emphasis on fatigue and fracture. The static mechanical properties were evaluated first, since they provide the guidelines needed to study the fatigue behavior. The first group of samples was taken out of sintered ZrN pellets with different amount of Palladium (Pd) added as a sintering aid. The relative densities of the samples were measured as well as hardness (Hv) and fracture toughness (K_{Ic}). Microstructural characterization revealed the presence of distributed porosity and microcracking in all samples. However, there was a clear tendency for these defects to decrease with added Pd. The microhardness measurement showed that a reduction in porosity and an increase in Pd content resulted in higher hardness and toughness, and the K_{Ic} for 5 wt% Pd was 50% higher than that of pure ZrN. However, the values of these parameters revealed that the material was intrinsically brittle ($K_{Icmax} \approx 3 \text{ MPa.m}^{1/2}$). Pure ZrN pellets prepared with an improved sintering process were then evaluated for hardness and toughness. The results indicated a slight increase of the properties with respect to the pure ZrN from the previous process. Fractography indicated that several fracture mechanisms, including microcrack/porosity linkage, cleavage and intergranular cracking, were active in all cases, and that an increase on the fraction of monolithic phases increased the mechanical properties. Material produced with the improved process was also heat treated at 800°C for 24 hours under high purity nitrogen, to estimate the effect that temperature might have on the structural stability of the material. It was found that the heat treatment resulted in improved static properties, since both the hardness and the fracture toughness increased with respect to the untreated specimens an average of 45% and 41%, respectively. The effect was attributed to an increase in the mechanical properties at grain boundaries.

The fatigue behavior was studied once the static properties were evaluated and notched samples were tested under four point bending at different levels of applied stress intensity range, from 30% to 87% of the measured fracture toughness. Fatigue lives were measured for these different conditions to evaluate the fatigue resistance. It was found that fatigue damage becomes accentuated when the applied loads approached a significant fraction of the fracture toughness, and that for applied stress intensities of less than 70% of K_{Ic} , the fatigue life of notched specimens can be more than one hundred thousand cycles. This is believed to be a result of the dominance of static failure modes during fatigue crack growth, which required stress intensities close to the fracture toughness of the material to occur. Fractography of specimens tested under cyclic loads indicated that the fracture mechanisms are similar to those observed during static fracture; however, the fracture surface is generally more tortuous than for fracture under static loads and material debris were also found, suggesting frictional effects during crack growth. Nevertheless, these results indicate that the fatigue behavior at low temperatures is directly linked to the toughness of the material. Hence, an increase in the fracture resistance of the material is likely to improve the fatigue behavior at room temperature. This behavior is expected to change under elevated temperatures, since other inelastic deformation mechanisms besides micro-cracking can be operational.

1. Experimental

Cylindrical ZrN pellets, 12 mm in diameter and approximately 3 mm thick, with different Pd contents, 0, 0.3, 1 and 5 wt%, were sintered at LANL. Samples for metallographic characterization and microhardness testing were cut from these pellets using Wire Electro-Discharge Machining (WEDM). These samples were first polished with SiC paper (600, 800 and 1200 grit) and then finished with 1 μm diamond paste. Samples for fracture toughness were also cut using WEDM, in the form of micro-beams with height and thickness of approximately 1 mm and lengths of about 6-7 mm. Notches with lengths of approximately one half of the height were also made using WEDM. The surfaces of these beams were polished with SiC paper only up to 1200 grit. Pellets produced with an improved procedure were also cylindrical, 12 mm in diameter and 12 mm in height. Samples were prepared with the same procedure mentioned above.

Hardness testing was carried out in a standard microhardness testing apparatus using a Vickers indenter (four-sided pyramidal diamond tip) with a load of 500 grs. Five indents were made per sample, in order to obtain average values of the hardness. Fracture toughness testing was performed using a screw-driven loading stage under displacement control following the procedures specified by the standard ASTM E-399. The load resulting in fracture was measured using a 500 lb load cell. Fatigue testing was performed using 4-point bending under load control in a servohydraulic Instron 1331 load frame. Load amplitudes were set to have a maximum K_I equal to a given fraction of the measured fracture toughness of the material and the minimum load was selected to have a load ratio ($R=L_{\min}/L_{\max}$) of 0.1. Cracks were nucleated from the notches using compression-compression loading, as described in [1].

Microstructural characterization, measurement of indents for hardness determination and fractography were carried using Scanning Electron Microscopy (SEM) in a JEOL JSM-840 equipped with an X-Ray detector for Energy Dispersion Spectroscopy (EDS). The microscope was run at a voltage of 20 kV. The relative density was measured by obtaining the volume fraction of porosity via analysis of the microstructure using image analysis software.

2. Results and discussion

2.1 Initial material

Mechanical Properties: The results from the microhardness and the fracture toughness experiments are plotted in Fig. 1, along with the relative density of the samples as functions of the Pd content. Note that both the relative density and the microhardness reach a local maximum between 0 and 1 wt% Pd, indicating that a reduction of porosity can lead, as expected, to an increase in the mechanical properties of the material. However, the value of hardness for this range of Pd content, about 320 Kg/mm², is relatively low as compared to other ceramics and nitrides, where it can reach more than three times this value. The presence of porosity is the most likely explanation for the low hardness. The high value of relative density and microhardness at 5% Pd confirms this trend. The fracture toughness did not present a local maximum between 0 and 1% Pd, suggesting that small additions of the sintering aid may in fact be detrimental for the fracture toughness.

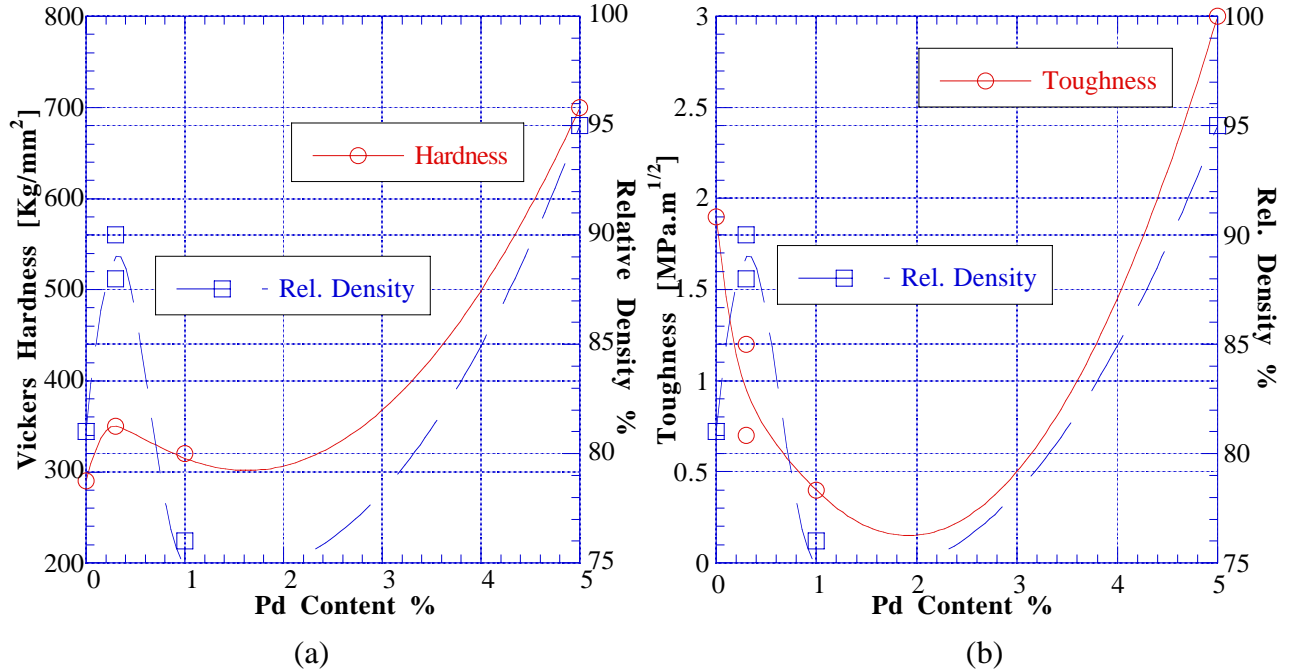


Fig. 1. (a) Hardness and (b) toughness as functions of the Pd content. Density is also shown.

However, a substantial increase in K_{Ic} was obtained at 5% Pd, where the highest density was obtained. The presence of a higher fraction of monolithic material can certainly account for this results, as will be shown in the next section. Microstructure characterization: the distribution of porosity is shown in Fig. 2.

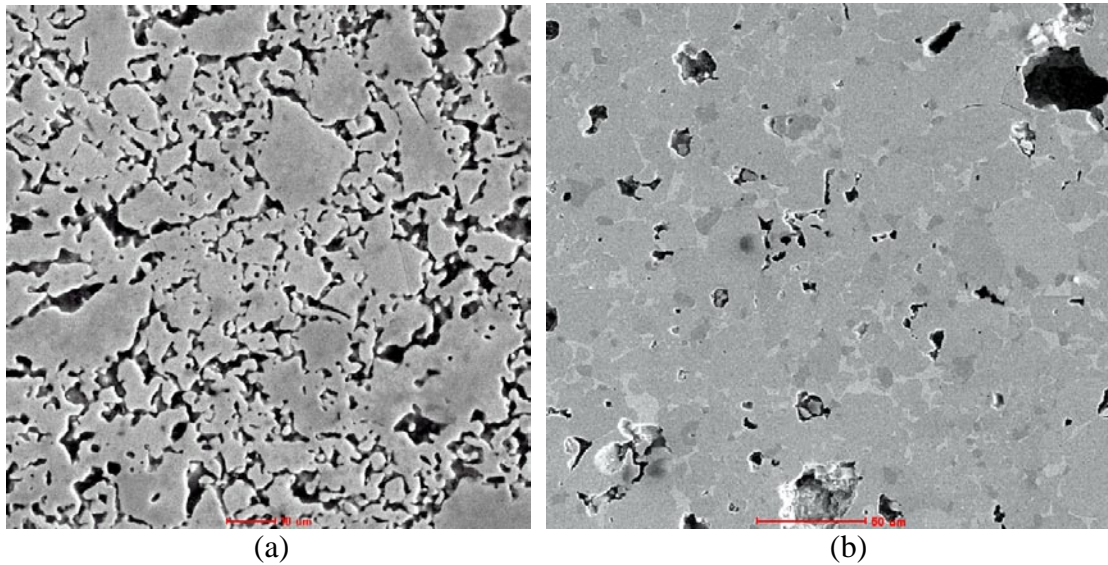


Fig. 2. Porosity distribution in (a) sample with 0 wt% Pd; (b) sample with 5 wt% Pd. The scale bar in (a) is 10 μm long, whereas the scale bar in (b) is 50 μm long.

Note that the porosity at low Pd content is small and well distributed, whereas the material with high Pd content has large regions seemingly free of porosity, which correlates well with the observed enhancement in mechanical properties. The micrograph shown in Fig. 2b also suggests

that a second phase might be present in this material. Hence, Backscattered Electron (BSE) images were collected using SEM in order to identify the presence of second phases due to the addition of Pd. In this sense, no second phase was detected in the sample with 0 wt% Pd and only a few small scattered particles were found in the specimen with 0.3 wt% Pd. The highest amount of second phase was detected in the sample with 5% Pd and this phase had the largest fraction of Pd. The EDS spectra corresponding to the matrix and the particles for this sample are shown in Fig. 3.

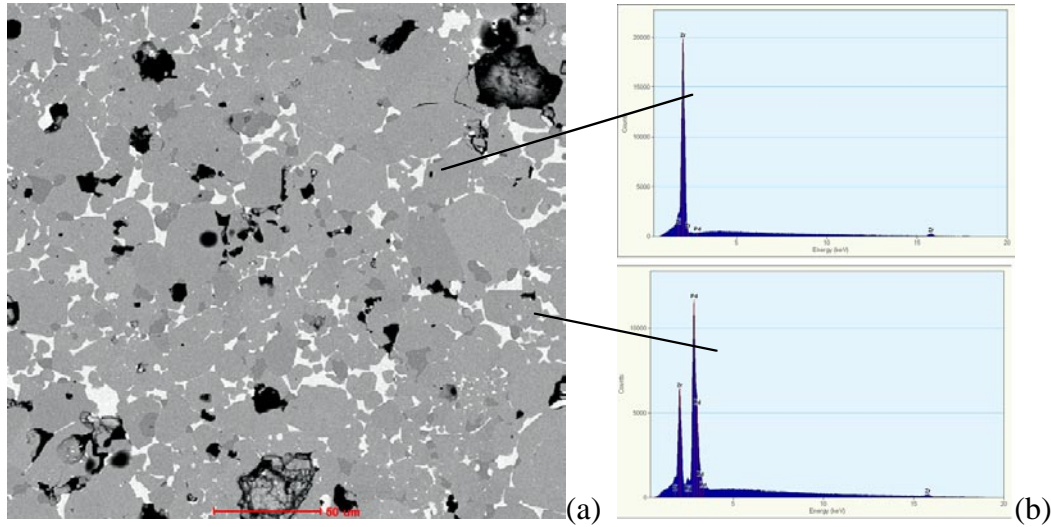


Fig. 3. (a) BSE image of the sample with 5% Pd, (b) EDS spectra for the matrix (top) and for the second phase (bottom). The micron bar in (a) is 50 μm long.

Fractography: the difference of approximately 40% in the fracture toughness of pure ZrN and the sample with 5 wt% Pd is likely to be meaningful in this case. In particular, the difference in the microstructure observed between these samples could have produced a change in the fracture mechanisms. Therefore, the fracture surfaces were examined using SEM. An image showing the fracture surface of the specimens with 0% and 5% Pd is shown in Fig. 4.

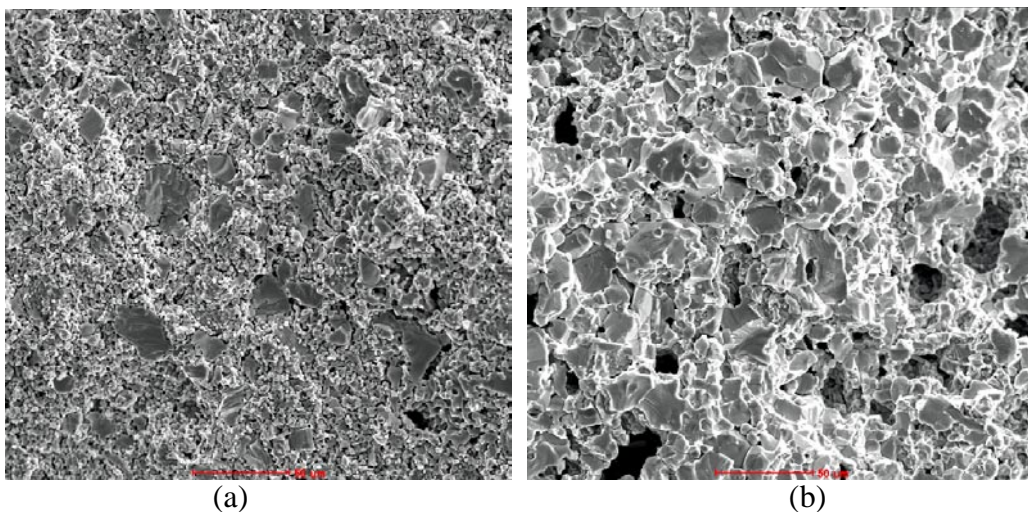


Fig. 4. Fracture surfaces of sample with (a) 0% Pd and (b) 5% Pd. The micron bars are 50 μm long.

A distinctive feature in the fracture surface shown in Fig. 4a is the presence of two components: a matrix with a high density of porosity and a number of particles embedded in it. The appearance of the matrix suggests that fracture in this part of the microstructure occurred due to linkage of pores and micro-cracks. The large particles, on the other hand, show an appearance typical of brittle fracture. In particular, the ridges that can be observed in some of them indicate that cleavage was operating in this case. The crack was quite flat at the macroscopic level, but it is obviously rough at the micro level. This may explain the value of fracture toughness obtained: $2 \text{ MPa}\cdot\text{m}^{1/2}$ is somewhat higher than what was initially expected, given the porosity present in the material. However, the crack deflections at the micro level, along with the fracture strength of the particles in the crack path, must have produced the level of toughness measured, which is similar to that of some monolithic ceramics. Regarding Fig. 4b, note that the fractions of porous matrix and monolithic particles are now almost opposite to those observed in Fig. 4a. It is clear from the picture that most of the cracking occurs across the particles themselves. Flat facets with and without ridges can be seen, suggesting brittle fracture due to cleavage and intergranular decohesion, respectively. The roughness of the fracture plane is also higher than in the previous case as can be seen in Fig. 5.

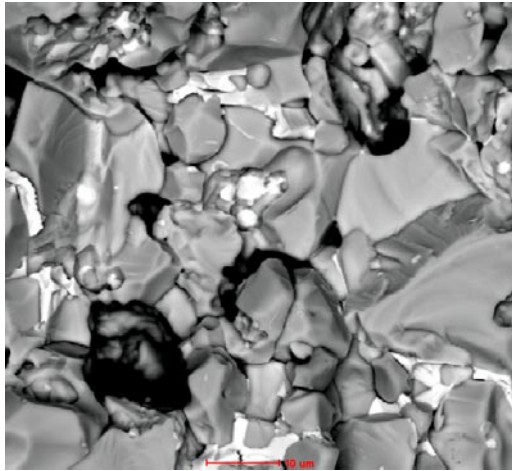


Fig. 5. BSE image of the fracture surface of a sample with 5% Pd. The micron bar is 10 μm long.

All these factors combined can explain the increased toughness of the material. In addition, the presence of a higher fraction of second phase, as found during the microstructural characterization, can lead

to larger values of toughness, due to the additional crack deflections when the crack propagates from one phase to another. Nevertheless, the second phase could also contribute to reduce the toughness if it were weaker than the matrix. In that case the fracture surface could show a higher fraction of second phase than the matrix. A BSE image of the fracture surface taken to elucidate this is shown in Fig. 5.

The bright particles in Fig. 7 are made of the Pd rich phase. The area fraction of these particles does not seem to be qualitatively higher than their fraction in the matrix. In fact, it seems to be qualitatively lower, suggesting that cracks may deflect to avoid the second phase. More studies are necessary to test this hypothesis. The image in Fig. 9 also shows quite clearly the ridges typical of cleavage and the flat facets that can usually be seen during intergranular fracture. This variety of fracture mechanisms can lead to toughening as observed in other ceramics, e.g., crack deflections due to differences in moduli and fracture strength between particles and grains can increase fracture resistance.

2.2 Material produced with an improved process

Mechanical Properties: The results from the microhardness and the fracture toughness experiments for samples with and without heat treatment are plotted in Fig. 6. Four different sample batches (3 to 6) are shown.

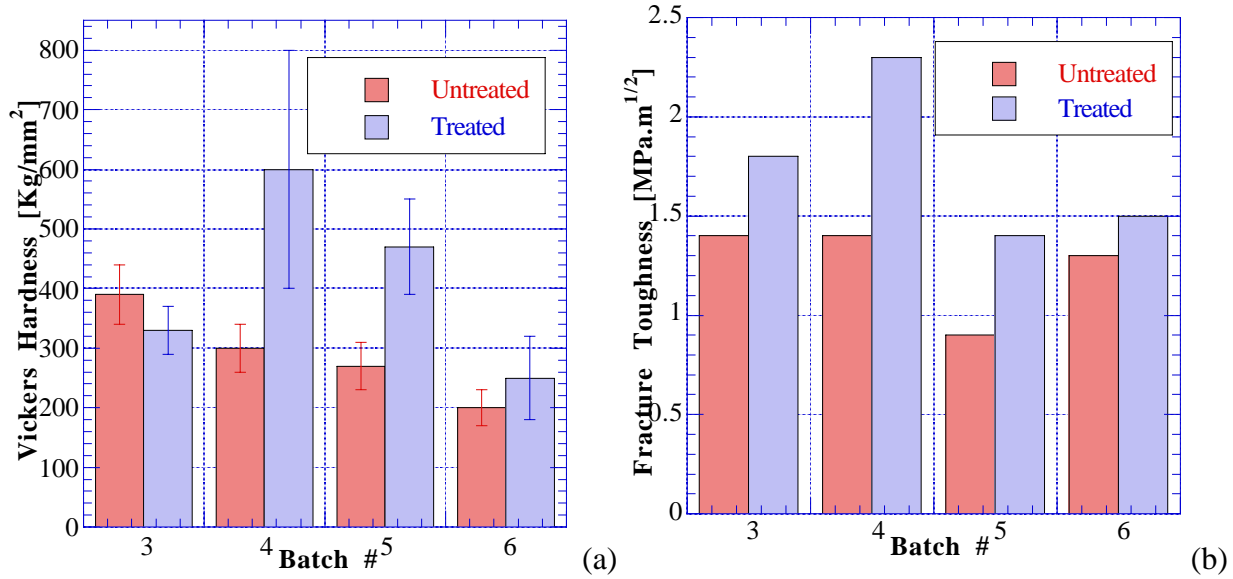


Fig. 6. (a) Hardness and (b) toughness as functions of the heat treatment.

Note that there is a measurable increase in the mechanical properties of the material in three out of four batches for the hardness and in all cases for the fracture toughness. The values of the mechanical properties for the untreated specimens did not correlate very well with the measured density, as was the case for the samples with Pd additions. The relative densities were 81% for batch 3, 94% for batch 4, 93% for batch 5 and 85% for batch 6. Densities measured via SEM images were about the same after heat treatment. However, note that the increase in properties correlates well with the initial density, i.e., samples with densities that were high initially (batches 4 and 5) have the highest increases on their measured mechanical properties after the heat treatment. This suggests that the new method to sinter the pellets can be optimized even further by using an adequate intermediate temperature for heat treatment after sintering at large temperatures. The fracture surfaces offered some insight about the reason for this increase (Fig. 7).

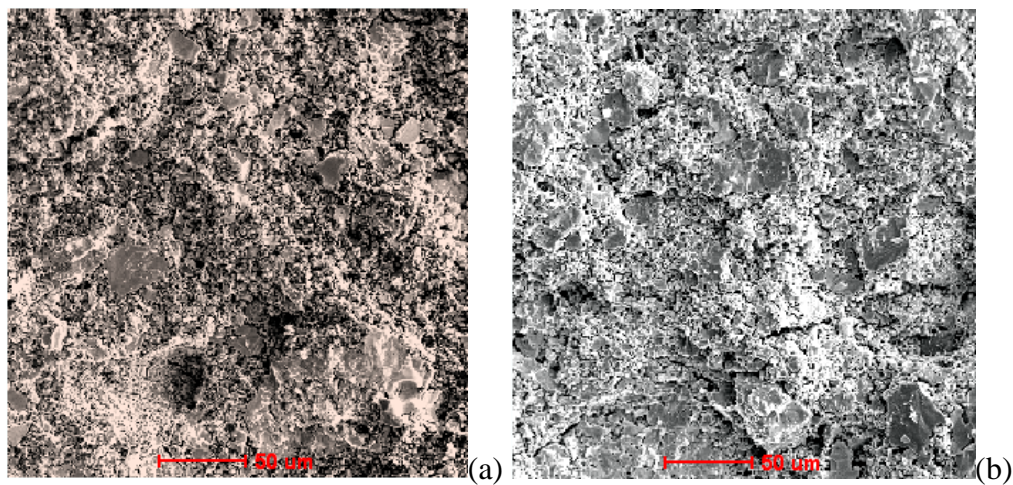


Fig. 7. Fracture surfaces for samples from batch 3; (a) before heat treatment; (b) after treatment.

It seems likely that the heat treatment improved the properties of interfaces between particles, probably by putting nitrogen in solid solution. This could not be verified using EDS in the SEM, since nitrogen is hard to quantify in the available microscope; however, a direct comparison of the fracture surfaces for samples before and after heat treatment offers some indirect evidence pointing along this direction. The comparison of these two fracture surfaces indicates that the crack in the treated sample had to propagate across particles, given the higher fraction of cleaved surfaces that can be observed in Fig. 7b. The fracture surface in the untreated sample shows a lower fraction of cleaved surfaces, indicating that the crack could propagate between particles. This, in turn, points to weaker interfaces in the untreated material. The maximum fracture toughness obtained in the heat treated specimens is higher than the toughness of the pure ZrN that was evaluated in the first part of this work (section 2.1). However, the variability of results, particularly with respect to the densities, indicates that further improvements to the sintering process are required in order to reduce the scatter and improve the structural reliability of the material.

2.3 Fatigue Behavior

Sharp pre-cracks were nucleated from notched specimens in compression-compression fatigue using four-point bending, as shown in Fig. 8.

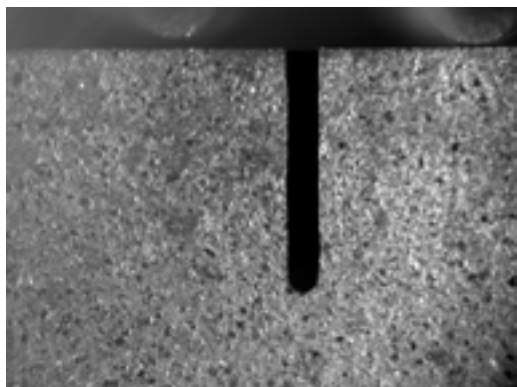


Fig. 8. Setup for nucleation of a crack in compression-compression fatigue. The width of the notch is approximately 0.2 mm.

It was found that load amplitudes of more than 50% of the estimated fracture toughness of the material were required to initiate a crack using compression-compression loading. In addition, cracks did not always nucleate at the tip of the notch. In at least two specimens sharp cracks nucleated from the side of the notch, just where the radius of the tip begins. These cracks eventually propagated to total failure. Once a crack of adequate length was nucleated, e.g., one or two times the width of the notch, the sample was flipped over to apply tension to the crack tip and proceed with fatigue test.

Samples for the fatigue test had dimensions consistent with ASTM E-399; however, the four-point bending setup used is not covered by the standard. This setup was chosen to insure a homogeneous loading in the region surrounding the notch, since four-point bending produces a constant moment in the central section of the beam. This, in turn, helps to decrease the scatter in the results. The load amplitudes used were chosen such that the maximum stress intensity applied were 0%, 43%, 58%, 72% and 87% of the maximum fracture toughness measured, which was estimated at $2.4 \text{ MPa}\cdot\text{m}^{1/2}$ for treated samples. These fractions were 3. The lives measured are shown in Table 1.

Table 1. Summary of fatigue behavior for the samples tested

Test #	Applied Load (% of K_{Ic})	Fatigue Life (cycles)
1	30%	> 250,000
2	43%	\approx 200,000
3	58%	\approx 170,000
4	72%	\approx 120,000
5	87%	\approx 700

The sample at the lowest load amplitude did not show signs of crack propagation after more than a quarter million cycles. The other samples did finally break, and in most cases the fracture surface was macroscopically perpendicular to the applied load. The one exception is sample five, the one tested at the maximum amplitude, where the crack propagated at an angle and ended on one of the load pins, probably because of local stress concentrations.

The sharp difference in fatigue lives between the 72% and 87% applied load indicates that the fatigue crack propagation in this material is controlled by static deformation modes, at least at room temperature. Note that the fatigue lives fall into the high cycle fatigue regime; however, the applied stress amplitudes are fairly low (the maximum was approximately $2.08 \text{ MPa} \cdot \text{m}^{1/2}$). Examinations of the fracture surfaces confirmed these observations. A typical fracture surface is shown in Fig. 9.

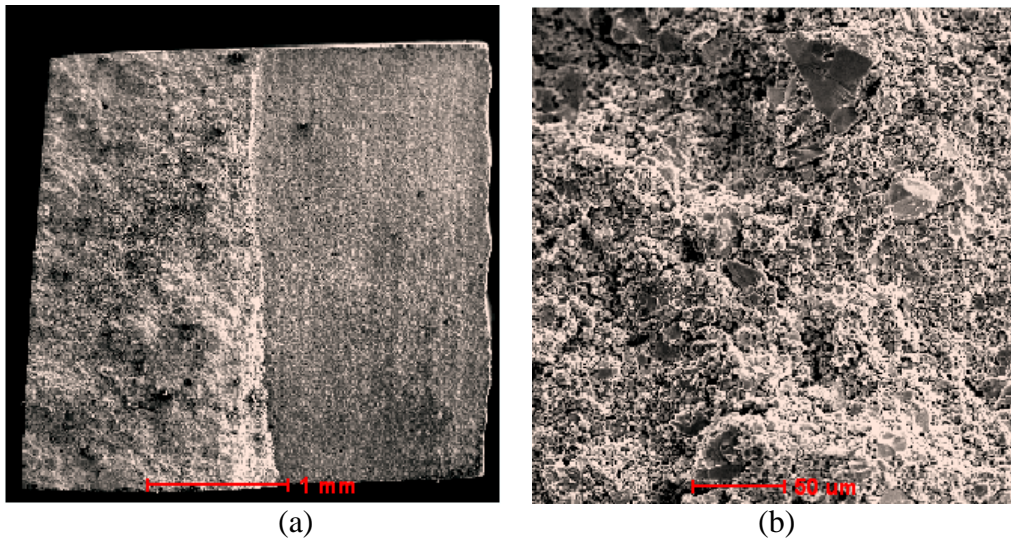


Fig. 9. Fracture surfaces of a sample tested at 72% K_{Ic} . (a) 80x; (b) 400x.

Note from Fig. 9a that there is a noticeable macroscopic roughness of the fracture surface, which is one of the differences observed with respect to fracture under monotonic loading. The aspect of the fracture surface at the microscopic level, Fig. 9b, shows that the same mechanisms observed during static fracture are present, namely, cleavage of particles and linking of microcracks. However, the presence of material debris was observed, which is compatible with rubbing and frictional processes during the growth of rough cracks in brittle materials. In this sense, the fatigue behavior of the ZrN pellets is consistent with what has been observed in many other ceramic materials, where failure modes can be mostly related to static deformation mechanisms and the presence of cyclic loading can lead to a resistance to crack growth due to frictional effects and the presence of crack tortuosity [1].

3. Conclusions

The preliminary assessment of the fatigue behavior and mechanical properties of sintered ZrN pellets leads to the following conclusions:

- a. There is an increase in hardness linked to an increase in relative density. It is likely that the presence of a higher fraction of particles of a Pd rich phase also induces an increase in the hardness in the material with Pd additions.
- b. Porosity is homogeneously distributed in samples with 1% Pd or less resulting in a low value of hardness. This situation changes dramatically in the sample with 5% Pd, where porosity with two distinct length scales can be observed. Samples produced with the improved sintering process showed large grains. Palladium additions should be considered as a way to improve the microstructure and mechanical behavior of sintered ZrN.
- c. Assessment of the fracture resistance of ZrN samples indicate that the sintered material has a toughness that is comparable to that of some monolithic ceramics, despite the large amount of porosity present. In addition, the material with 5% Pd showed an estimated value of toughness 50% higher than that of pure sintered ZrN.
- d. Fractographic studies of the broken specimens indicate that a variety of fracture mechanisms are active during cracking of the materials tested. In particular, porosity linkage and cleavage seem to dominate for samples without sintering aid, whereas cleavage and intergranular fracture are more evident for samples with 5% Pd. Crack deflection and an increase in fracture strength due to the presence of a higher fraction of monolithic particles can explain the higher value of fracture toughness measured in the sample with 5% Pd.
- e. Heat treatment of samples at intermediate temperatures can increase their mechanical properties, probably by improving the fracture resistance of material in between sintered particles.
- f. Fatigue behavior of the ZrN pellets can lead to fatigue lives of more than 250,000 cycles for low values of the applied loads.
- g. Dramatic changes in the fatigue behavior are observed when the applied loads are a significant fraction of the fracture toughness of the material. The accelerated crack propagation and failure indicates that static failure mechanisms control the fatigue behavior at low temperatures.
- h. The study of the fracture surfaces of fatigue specimens showed that crack tortuosity and frictional effects may play a role during fatigue crack growth in sintered ZrN. These effects are likely to lead to some of the crack growth resistance needed to propagate fatigue cracks in ceramic materials.

4. References

1. S. Suresh, *Fatigue of Materials*. Second ed. 1998, Cambridge. Cambridge University Press.